6 Head-Tail Instability in Tevatron

Tevatron performance has been suffering from a coherent transverse instability for quite long time. The instability was a concern for Run 1b and is still one of the main limitations of proton bunch intensity. In order to prevent the instability for the high intensity proton beam, the Tevatron lattice chromaticities should be set above 8 at the injection (150 GeV) and above 26 at the collision energy (980 GeV). Although this suppresses the instability, it results in a degradation of machine performance due to the reduction of beam lifetime. The observation of particle loss in the vicinity of CDF-detector clearly demonstrates that minimum loss is achieved at zero chromaticity[1], and that loss increases with the growth of its absolute value. This stimulated us to investigate a driving mechanism for this instability, as well as to search for possible solutions to operate at zero chromaticities. The measurements performed in November 2002 exhibited that the transverse impedance significantly exceeds the Run II transverse impedance budget[2]. The source of the excessive impedance was tracked to two laminated lambertson magnets. The removal one of them[6] at the January 2003 shutdown significantly reduced the chromaticities required for the beam stabilization. This summer we plan to insert a shielding liner into the remaining injection lambertson magnet.

6.1 DIRECT INSTABILITY OBSERVATIONS

A fast digital oscilloscope, connected to the horizontal and vertical 1-meter long strip-line pickups, records turn-by-turn data for 2000 turns. Data for each turn are sampled during 80 ns with 0.4 ns rate so that the transverse head-tail dynamics of a single bunch could be observed. During data analysis both the sum and difference signals are deconvoluted. Deconvolution of the sum signal represents the particle distribution along the bunch, while deconvolution of the difference signal represents the dipole moment along the bunch. Figure 1 depicts the unprocessed sum and difference signals and their deconvolution.

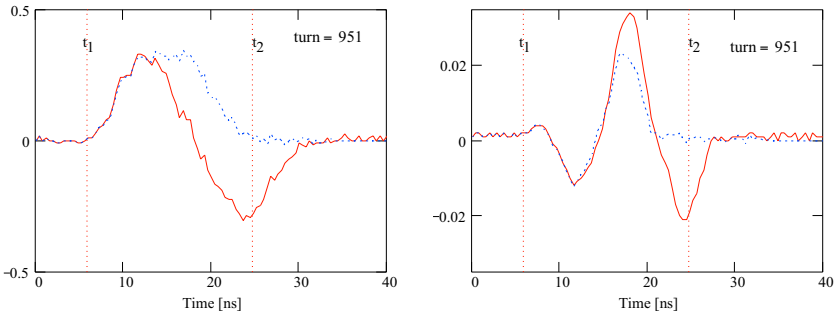

Figure 1. Unprocessed sum (left) and difference (right) signals of the vertical pickup and their deconvolution for turn 951. Measurements are performed before C0 lambertson magnet removal. Solid lines – unprocessed signals, dashed lines – deconvolution of the signals. The lattice chromaticities ($pd\nu/dp$) are: ν'_x = -1.75, ν'_y = -3.5; bunch population - $2.6 \cdot 10^{11}$. Vertical lines show boundaries of the RF bucket.

[6] C0 lambertson was earlier used for slow beam extraction from Tevatron. It has not been required for the Run II collider operation but presented a tight vertical aperture limitation and made a large contribution to the ring transverse impedance.

Measurements are synchronized with beam injection. Chromaticities are set below zero so that the mode l=0 would be unstable. Figure 2 presents turn-by-turn positions separated in time by about a quarter of synchrotron oscillation before C0 lambertson removal. Figure 3 presents dependence on time for vertical and horizontal betatron amplitudes averaged along the bunch. Strong coupling between vertical and horizontal degrees of freedom results in the oscillations of the amplitudes with period about 57 turns. In average the amplitudes exponentially grow with increment of 115±5 s^{-1}.

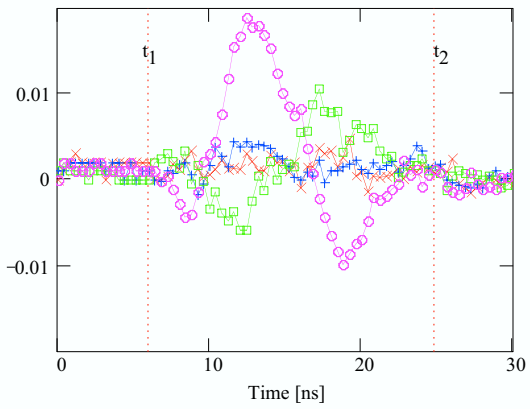

Figure 2. Turn-by-turn dipole moments along the bunch for the same measurements as presented in Figure 1. Curves are separated in time by 301 turns (about quarter of synchrotron oscillation).: × - turn 0, + - turn 301, □ - turn 602, ◇ - turn 903.

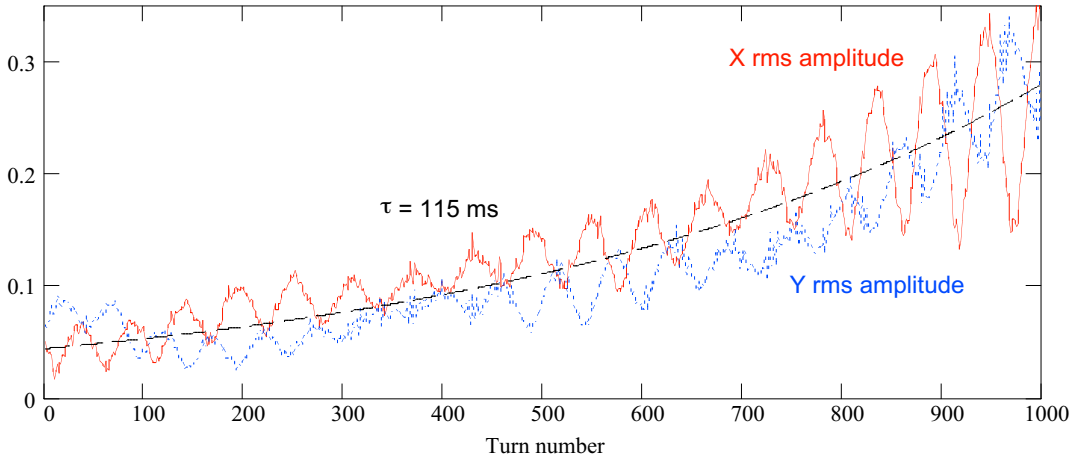

Figure 3. Dependence on time for the betatron amplitudes averaged along the bunch for Figure 1 parameters.

Turn-by-turn beam position measurements performed in the absence of instability show that the vertical mode is strongly coupled so that the vertical and horizontal motions for this mode have approximately the same amplitudes on the head-tail monitor. Coupling for the horizontal mode is significantly smaller and the motion occurs mainly in the horizontal plane. Taking this into account we conclude that the data presented in Figure 3 represent a development of the head-tail instability for vertical betatron mode.

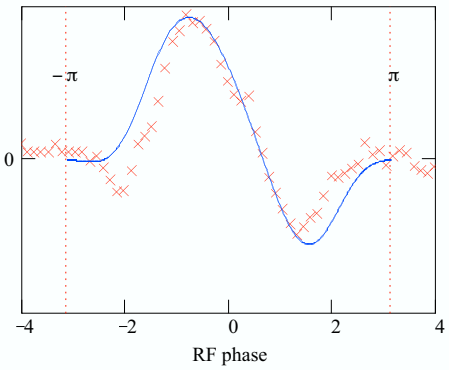

Figure 4. Fitting measured data (turn 903 of Figure 2) to the air-bag beam model in the absence of interaction with chromaticity ν_y'=-3.2.

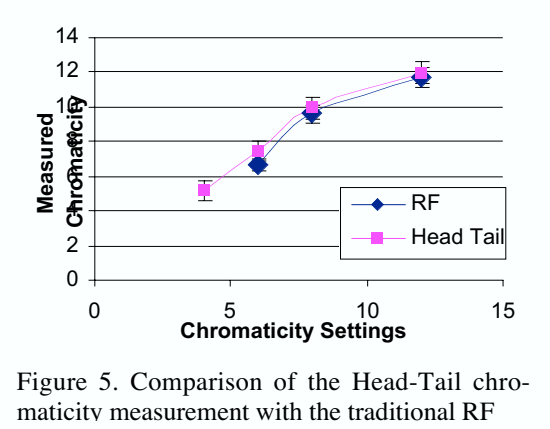

Figure 5. Comparison of the Head-Tail chromaticity measurement with the traditional RF

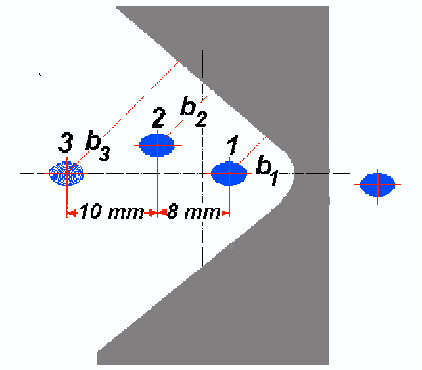

Figure.6. Layout of the local orbit bumps used in Figure 7.

The measurement verified that the instability has a monopole longitudinal configuration (l = 0) as it is expected for negative chromatisity. Figure 4 presents a comparison of the measured dipole moment and the prediction of the air-bag model in the absence of interaction for l = 0. Chromaticity used in the fitting (ν_y' = -3.2) coincides with its direct measurement (ν_y' = -3.5) within measurement accuracy.

To crosscheck the measurements we also measured the chromaticity by pinging the beam and measuring the phase shift between the head and tail in the absence of instability. The chromaticity was calculated from this phase difference according to Reference [3]:

$$\nu'_{x,y} = -\eta \frac{\Delta\Psi_{x,y}}{\omega_0 \Delta\tau \left(\cos\left(2\pi n \nu_s\right) - 1\right)} \quad . \tag{1}$$

Here $\Delta\Psi$ is the head-tail phase difference, η is the slip factor, ω_0 is the revolution frequency, ν_s is the synchrotron frequency, and $\Delta\tau$ is the time length of the bunch. Figure 5 presents comparison of the chromaticities measured directly and by the head-tail technique.

The development of instability caused a reduction of bunch intensity with consequent change of betatron tune, which allowed us to determine the coherent tune shift. Its value $\Delta\nu$=0.0011±0.0001 is smaller than the synchrotron tune, $\Delta\nu \approx 0.7\nu_s$. This classifies the instability as the weak head-tail instability.

6.2 TRANSVERSE IMPEDANCE ESTIMATE

To compute the transverse impedance accurately we built a computer model of the instability. An ensemble of macro-particles with the Gaussian longitudinal distribution has been tracked many turns for particles interacting through the resistive wake field. The Landau damping was not taken into account in the model, and therefore matching the measurements and simulations yields the low boundary for the transverse impedance. The measurements were performed at the injection orbit where the growth rate is ≈120 s^{-1}. That results in $Z_{\perp\min} \approx$ 4-5 MΩ/m.

The Tevatron stainless steel vacuum chamber has a square cross section with $2h$ = 6 cm. Its transverse impedance amounts to ~0.9 MΩ/m at 100 MHz[2]. That is about 5 times smaller than the measured value. After careful examination it was suggested that a major source of impedance is the lambertson injection magnet. Its value can be estimated by integrating the resistance over the low frequency current passing through the

laminas[4]:

$$Z_{\perp} \approx \frac{2Z_o}{\pi\, b^2} \cdot \frac{\mu}{\kappa} \cdot F \cdot \frac{L}{d} \quad , \qquad (2)$$

where $\kappa^2 = -4\pi i\sigma\mu\omega / c^2$, $Z_0 \approx$ 377 Ω, $\mu \approx 100$, $F \approx 0.5 - 1$ is a geometry form-factor, $L = 11.2$ m is a total length of the magnet, and $d \approx 1$ mm is the lamination thickness.

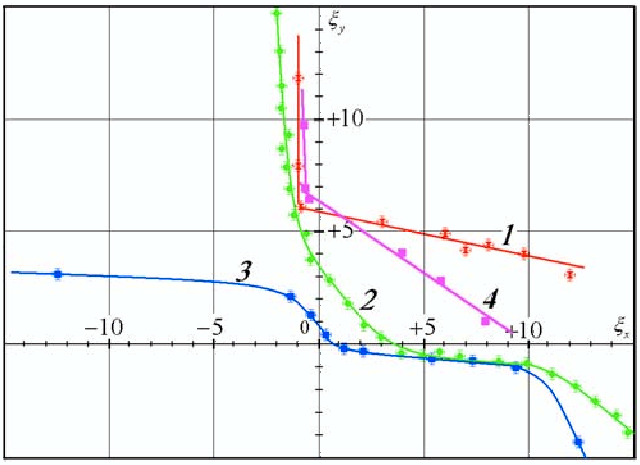

Figure 7. The stability regions for the head-tail modes in the chromaticity space. All measurements are performed with single proton bunch (Nppb=2.65·10[11]). The thresholds of the excitation correspond to an increase in the coherent component of the Schottky spectrum as the chromaticities were smooth decreased. Curves 1-3 correspond to the orbit positions presented in Figure 5. Curve 4 corresponds to the same position as curve 2 but has been taken before C0 lambertson removal.

6.3 Stability bounds

As can be seen in Figure 7, the stability bounds in the chromaticity space have been extended after C0 lambertson magnet removal. To prove that the remaining injection lambertson magnet makes a dominant contribution to the transverse impedance, the stability bounds were measured for the three local beam orbit offsets (see Figures 6 and 7). As one can see, the beam displacement in the magnet strongly affects the stability bounds. Using Eq. (2) one can find the following values for the lambertson magnet transverse impedance at different locations inside the magnet: (1) injection local orbit bump, $b_1 \approx 6$ mm, $Z_{\perp} \approx 5$ MW/m; (2) central regular orbit, $b_2 \approx 9$ mm, $Z_{\perp} \approx 1.8$ MW/m; (3) local orbit bump with respect to the central orbit, $\Delta Y = -3$ mm, $\Delta X = -10$ mm, $b_3 \approx 18$ mm, $Z_{\perp} \approx 0.6$ MW/m.

At both positive and negative chromaticities the betatron mode corresponding to the vertical motion is less stable than the horizontal mode. At positive chromaticity the stability is limited by excitation of the quadrupole mode with longitudinal number *l=2* (see Fig. 8) while the coherent mode with the monopole longitudinal configuration *l=0* limits stability for negative chromaticities.

The Tevatron tunes ν_x=20.585 and ν_y=20.575 are located in vicinity of the coupling resonance $\nu_x - \nu_y = 0$. At crossing the resonance both the vertical and horizontal coherent modes become unstable that can be caused by a repartition of the direct space-charge tune shift between two normal betatron modes with the coupling increased.

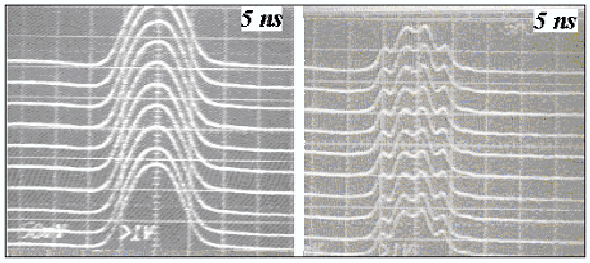

Figure 8. Longitudinal density profiles of the initial (N_{ppb}=2.65·10[11]) and remaining ((N_{ppb}=1.03·10[11]) proton bunches before and after self-stabilization of the vertical instability due to the particle losses. The particles were lost in accordance with the longitudinal configuration of the coherent vertical oscillations that points qualitatively at excitation of the head-tail mode with ***l=2***

6.4 SPACE CHARGE EFFECT

Horizontal and vertical impedances of lambertson magnet as well as the

resistive wall impedance of the Tevatron vacuum chamber are close, but as can be seen in Figure 7 the stability bounds for the vertical and horizontal modes are quite different. A possible reason could be related to the space charge tune shifts, which are different for the two planes because of dispersion. The vertical incoherent shift is two times larger than the horizontal shift. Coherent tune shifts for the first two horizontal modes are calculated to be comparable with the incoherent space-charge tune shift that promotes Landau damping due to a synchrotron tune spread. The vertical modes are in a worse condition because the space-charge shift is higher.

At Tevatron injection energy the synchrotron tune and rms-synchrotron tune spread are: $\nu_s \approx 1.8\cdot10^{-3}$, $\delta\nu_s \approx 2.2\cdot10^{-4}$. For the 3D-Gaussian charge distribution the linear space charge tune shifts are:

$$\Delta\nu_{x,y}^{sc} = -\frac{N_{ppb}\, r_0\, R_0}{\sqrt{2\pi}\,\beta^2\gamma^3\sigma_z}\left\langle \frac{\beta_{x,y}}{\sigma_{x,y}\left(\sigma_x+\sigma_y\right)}\right\rangle \quad , \tag{3}$$

where $\sigma_{x,y}(s) = \sqrt{\varepsilon_{x,y}\beta_{x,y}(s) + D_{x,y}^2(s)\sigma_{\Delta p/p}^2}$ are the transverse beam sizes, $\langle\cdots\rangle$ means averaging over the machine. For bunch intensity of $2.6\cdot10^{11}$ and σ_s = 90 cm it yields $\Delta\nu_x^{sc} \approx -0.36\cdot10^{-3}$ and $\Delta\nu_y^{sc} \approx -0.7\cdot10^{-3}$. Laslett tune shifts due to electric- and magnetic-image fields are negligible compared to contribution of the electromagnetic self-fields and therefore are omitted.

6.5 DAMPING OF THE HEAD-TAIL MODES BY CUBIC NON-LINEARITY

Presently, in order to work at decreased chromaticities ($\xi_x \approx 6$, $\xi_y \approx 4$), transverse dampers are used to prevent an excitation of transverse instability at the multi-bunch mode of operation[7]. A universal method for damping the instability is introducing a betatron frequency spread larger than the growth rates. Landau damping is effective when the coherent tune is within a band of incoherent tunes.

Two Tevatron regular octupole families are used to provide Landau damping for the head-tail modes: $OZD\left(n=12,\ \beta_x > \beta_y\right)$, $OZD\left(m=24,\ \beta_y > \beta_x\right)$. There are two sources of the octupole-driven tune spread: due to the betatron amplitudes and due to dispersion in the octupole locations.

$$\delta\nu_{x,y}^{\beta} = \frac{1}{16\pi\, B\rho}\left[J_{x,y}\sum_1^{n,m}\left(\overline{K}_3\beta_{x,y}^{\,2}\right)_{n,m} - 2J_{y,x}\sum_1^{n,m}\left(\overline{K}_3\beta_x\beta_y\right)_{n,m}\right] \quad , \tag{4}$$

$$\delta\nu_{x,y}^{D} = \frac{\sigma_{\Delta p/p}^2}{16\pi\, B\rho}\sum_1^{n,m}\left(\overline{K}_3\,\beta_{x,y}\,D_x^2\right)_{n,m} \quad , \tag{5}$$

where $J_{x,y} = a_{x,y}^2/\beta_{x,y}$ are single particle Courant-Snyder invariants and

$$\overline{K}_3(n,m) = I_{n,m}(Amps)\cdot\int_0^{L_0}\frac{\partial^3 B_y}{\partial x^3}ds \,/\, 1\,Amp \quad \left[T/m^2\right]$$

are the normalized octupole strengths with I_n, I_m as the OZF- and OZD-family octupole currents. On the central orbit, damping the vertical mode l=1 requires currents $I_{OZD} \approx 4.2\,A$ and $I_{OZF} = 0$ with the estimated tune spreads: $\left\langle\delta\nu_y^{Oct}\right\rangle \approx 0.28\cdot10^{-3}$, $\left\langle\delta\nu_x^{Oct}\right\rangle \approx 1\cdot10^{-4}$. At the chromaticity of $\xi_{x,y} \cong -2$ the coherent mode l = 0 has been stabilized at $I_{OZD} \approx 5\,A$ and $I_{OZF} \approx 2\,A$ with $\left\langle\delta\nu_y^{Oct}\right\rangle \approx 0.52\cdot10^{-3}$, $\left\langle\delta\nu_x^{Oct}\right\rangle \approx 0.38\cdot10^{-3}$.

In both cases the widths of betatron spectra measured by Schottky monitor are in reasonable agreement with this calculation, taking into account the contributions from the synchrotron and direct space-charge tune spreads. The octupole cubic non-linearity has the positive sign to minimize its affect on the dynamic aperture since the vertical tune is only slightly above the resonance $\nu_y = 4/7$. Besides, it has "right" sign to minimize the octupole strengths of the *OZD*-family.

CONCLUSION

The observed single-bunch head-tail instability was found to be driven mainly by the resistive impedance of laminated lambertson magnets. To reduce it we removed one of the magnets and plan to insert a thin shielding liner inside another magnet. It is expected to stabilize the higher order head-tail modes at positive chromaticities and significantly reduce the growth time at negative chromaticities.

Landau damping through the octupole-generated betatron tune spread for all of the unstable head-tail modes at positive and negative chromaticities has been verified. If reduction of the impedance will not be sufficient to stabilize the instability at chromaticities cloze to zero we plan to introduce octupole non-linearity in the routine machine operation.

REFERENCES

[1] X. Zhang, et al., Experimental studies of beam-beam-effects in Tevatron, PAC 2003.
[2] Tevatron Run-II Handbook, FNAL 1998.
[3] D. Cocq et. al., The measurement of chromaticity via a head-tail phase shift, BIW98, Stanford CA, 1998.
[4] A. Burov, V. Danilov, unpublished note, 2003.
[5] A.W. Chao, Physics of Collective Beam Instabilities in High Energy Accelerators, John Wiley&Sons, New York, 1993
[6] D.Mohl, Part.Acc.,v.50, p.177, 1995.
[7] C.Y. Tan, J. Steimel, The Tevatron Transverse Dampers, PAC 2003.

7 Beam-Beam Compensation

To evade the effects of beam-beam interactions and hopefully lead toward higher beam intensities two direct-compensation schemes are being investigated. The first employs one or more pulsed electron beams through which the antiproton bunches can pass. A prototype system, the Tevatron Electron Lens, has been installed in the Tevatron and continues to be studied. The second type of compensation technique uses a set of current-carrying wires near to and running parallel to the antiproton beam that produce forces on the beam resembling the long-range forces produced by the passing proton bunches. Such a system has been proposed for the Large Hadron Collider and subsequently a first look at the use of similar devices on the Tevatron beam has been undertaken.

7.1 Tevatron Electron Lens

The TEL can be used in principle to help compensate for the head-on tune shift caused by the beam-beam interactions at the detectors. Two such systems are required for beam-beam tuneshift compensation in both transverse degrees-of-freedom. Such systems can also be used to alleviate nonlinear tune-spread within each antiproton bunch by using electron beams with suitable transverse profiles.

Early results with the Tevatron Electron Lens have been reported elsewhere.[1] Tune shifts due to the lens have been observed and are consistent with expectations. The electron lens has become part of the routine Tevatron operation, but unfortunately for use as a beam cleaning device. During the past 1-2 years it has been run in a mode whereby it excites betatron oscillations of particles which find themselves within the abort gap, thus preventing magnet quenches during the extraction of beam from the Tevatron. Dedicated study time for the system's use for beam-beam compensation has been limited, but will continue to be pursued.

7.2 Wire Compensation of Long-range Beam-beam Effects

The idea of compensating the long-range beam-beam effects with current carrying wires was considered recently for the LHC [1]. The principle is simple; the strong beam can be regarded as a current, and its effect on the weak beam can be alleviated by another current placed in such a way that the fields cancel each other at the weak beam. The advantage is the simplicity of the method and the ability to deal with all multipole orders at once.

[1]See, for example, V. Shiltsev, et al., "First Experiments with Electron Lens for Beam-Beam Compensation in Tevatron," FERMILAB-Conf-01/390-T, Fermilab; V. Shiltsev, et al., 'Beam-Beam Compensation in Tevatron: First Results," PAC 2001, Chicago, IEEE-01CH37268, p. 154 (2001).

We choose to implement the wire as a transfer map which can be used by differential algebra codes such as Cosy Infinity. The first step is to look at the equations of the motion due to the integrated magnetic field of *a finite length* of straight wire at an arbitrary point in space.

7.2.1 Magnetic field and the map of a finite length wire

In canonical coordinates $\left(x, a=\frac{p_x}{p_0}; y, b=\frac{p_y}{p_0}\right)$, where p_0 is the momentum of the reference particle, the equations of the motion take the following form (assuming no longitudinal fields):

$$x^{'}=\frac{a}{\sqrt{1-a^2-b^2}},\quad y^{'}=\frac{b}{\sqrt{1-a^2-b^2}},\qquad a^{'}=-\frac{B_y}{(B\rho)},\ b^{'}=\frac{B_x}{(B\rho)}, \tag{1}$$

where $(B\rho)$ is the magnetic rigidity of the reference particle. The first two equations are the equations of the drift, while the last two are the equations of a kick. This leads to a second order symplectic integration of the system by an operator splitting method (which is equivalent to the so-called thin lens approximation), i.e. if the transfer map of a wire, embedded in a drift of length L, is denoted by $\mathcal{M}_w$, the map of the drift by $\mathcal{M}_d$, and the map of the kick by $\mathcal{M}_k$, the relation between them is

$$\mathcal{M}_w^{(L)} =_2 \mathcal{M}_d^{(L/2)} \circ \mathcal{M}_k^{(L)} \circ \mathcal{M}_d^{(L/2)}.$$

The solution for the kick is given by

$$a_f = a_i - \int_{-L/2}^{L/2} \frac{B_y}{(B\rho)} dz,\qquad b_f = b_i + \int_{-L/2}^{L/2} \frac{B_x}{(B\rho)} dz. \tag{2}$$

Therefore, to compute the kick one needs the integrated field generated by the wire. We note that this approach takes into account the wire's fringe field region too.

The magnetic field can be computed using the Biot-Savart law. Assume that in an arbitrary coordinate system (x, y, z) we have a wire of length l, such that the start of the wire is at a distance $\vec{r}_P$ from a point P where we want to compute the field. If the length of the wire is parametrized by λ such that $\vec{l}(\lambda) = \lambda\vec{l}$ with $\lambda \in [0, 1]$, the field, integrated over L, is given by

$$\left\langle \vec{B}_P \right\rangle = \frac{\mu_0}{4\pi} I \int_0^1 d\lambda \int_{-L/2}^{L/2} \frac{\vec{l} \times \vec{r}_P}{\left|\vec{r}_P - \lambda\vec{l}\right|^3} dz, \tag{3}$$

where I is the current.

The integrals can be done analytically. However, they simplify if the coordinate system is assumed parallel to the wire, that is, if $\vec{l} = (l_x, l_y, l_z)$, the coordinate system is oriented such that $l_x = l_y = 0$. In this case the result is given by

$$\left\langle \vec{B}_P \right\rangle = \frac{\mu_0}{4\pi} I \frac{\sqrt{\left(\frac{L}{2}+l\right)^2 + x^2 + y^2} - \sqrt{\left(\frac{L}{2}-l\right)^2 + x^2 + y^2}}{x^2 + y^2} \begin{pmatrix} x \\ y \\ 0 \end{pmatrix}. \tag{4}$$

Here x and y are regarded as the sums of the wire distance from the longitudinal axis and the particle's betatron amplitude. In case the wire is tilted with respect to the coordinate system, first the tilt of the coordinate system is performed, then the map of the wire applied.

Combining the maps of the pieces we can get the full transfer map of the wire, which allows for arbitrary length, current and placement, including pitch and yaw. It is given by

$$\mathcal{M}_w = \mathcal{S} \circ \mathcal{T}^{-1}_{\theta_x,\theta_y} \circ \mathcal{M}_d^{(L/2)} \circ \mathcal{M}_k^{(L)} \circ \mathcal{M}_d^{(L/2)} \circ \mathcal{T}_{\theta_x,\theta_y}, \tag{5}$$

where $\mathcal{T}_{\theta_x,\theta_y}$ represents the tilt of the coordinate system by horizontal and vertical angles θ_x, θ_y to orient the coordinate system parallel to the wire, and $\mathcal{S}$ represents a shift of the coordinate axes to make the coordinate systems after and before the wire agree.

7.2.2 Resonance compensation

At injection energy there are long-range interactions at 138 different locations, spread all over the circumference of the ring and phase space. There is practically no possible way to correct each interaction with an individual wire. We are also limited by the small number of drift spaces where wires could be installed.

As a first step in this study we looked at a set of four wires, placed in drifts that are at least 1 m long, where the horizontal and vertical beta functions are not too different, where the proton and antiproton closed orbits are well separated (in order for the wire to not affect the proton beam), and at a reasonable distance from the beam pipe. The wire needs to be at some comfortable distance from the antiproton beam to allow for orbit drifts and manipulations. We chose to focus on resonance strengths as a criterion for correction. The long-range beam-beam interactions drive mostly seventh order resonances at injection, with the $(3, 4)$ resonance dominating, making it a natural candidate for correction by wires.

The wires have been installed at the following sections: A17, F0, E0, and C0. The length of the wires was fixed to 1 m. To obtain a rough estimate for the current in the wires, we assumed round proton beams with design parameters and that the beam-beam kicks add up linearly. This leads to

$$I_w = (\frac{r_p m_p c^2}{0.2998}) N_b \times 10^7 = 12.89[\text{Amp}] \tag{6}$$

per interaction, where $N_b = 2.7 \times 10^{11}$ is the number of protons per bunch. This multiplied by 72 (interactions) / 4 (wires) gives $I_w = 232$ A in each wire. This is a large current and the wire may require cooling, as also envisaged for the LHC. Since the wire is placed on the side of the antiproton beam that is opposite to the proton beam, the sign of the current should be in the direction of the proton beam. These constraints fix the longitudinal positions, length, and currents. There is no obvious constraint that fixes the transverse positions. If there were one wire per interaction it is obvious that for the correction to not depend on the particle amplitudes, the wires should be placed at the same distance from the antiproton beam as the proton beam is from the antiproton beam. In our case with 72 interactions per

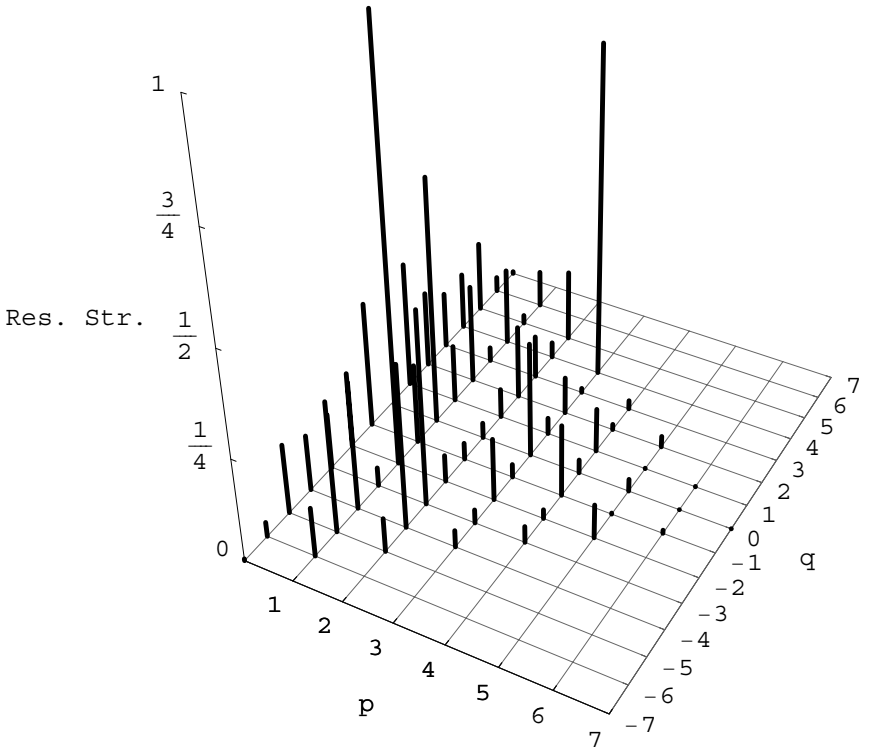

Figure 5: Resonance strengths at injection generated by the wires placed at a 45° angle in the $x - y$ plane.

bunch (and varying separations) and only four wires, there is no such clear criterion. From the map of the wire it is clear that by changing the antiproton beam - wire distance, or even the orientation of it, the map will be different, and might drive different resonances.

Indeed, the resonance structure changed with the transverse placement in simulations. Here we present some preliminary results. In the first set of runs we fixed some high currents and distance of the wires from the antiproton beam to 10 mm, and varied the orientation in the first quadrant, namely at angles 0°, 22.5°, 45°, 67.5° and 90° with respect to the horizontal. We computed the resonances up to order seven. Figure 5 shows the resonance structure when the angle was fixed at 45°. The $(3, 4)$ resonance is strongly driven at this angle.

In another simulation, we kept the angle of the wire the same as the plane of the helix but varied the distance of the wire from the anti-proton beam. If the wires are too far, the resonance structure in this geomery did not resemble the one generated by the beam-beam interactions. However as the distance decreased, the resonance structures become more alike with mostly the seventh order resonances driven. It is clear nonetheless that the resonance structure depends sensitively on the exact placement of the wire and a more robust compensation is necessary.

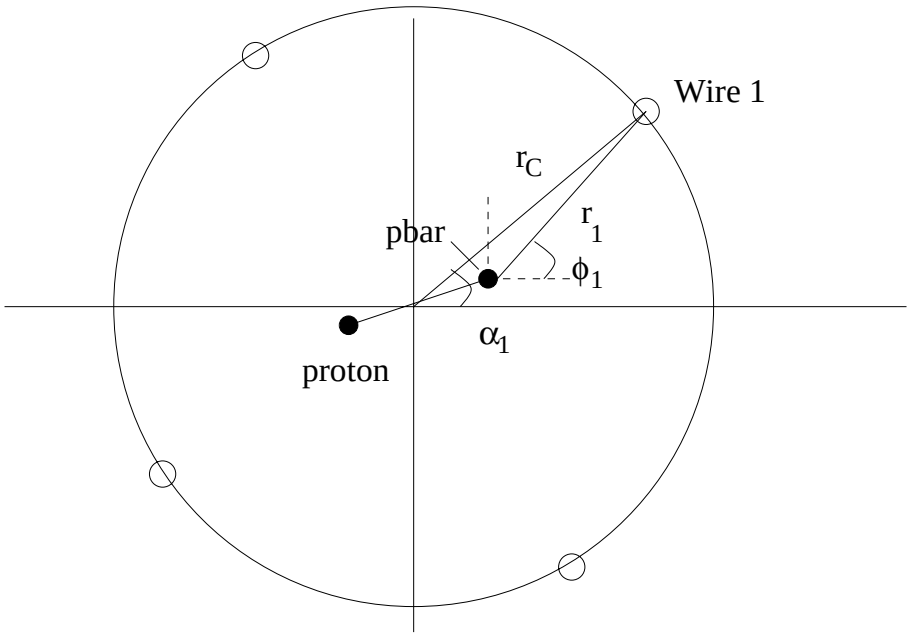

Figure 6: Cross section of the wire cage showing the wires placed on a circle of radius r_C with the 1st wire at an angle of α_1 w.r.t the x axis.

7.2.3 Multiple wires at a single location

One way to increase the robustness and flexibility of the compensation method is to place several wires around the circumference of a cylindrical cage at each location [2]. We consider here the fields produced by such a structure.

For simplicity we assume that the wires are infinitely long and each carries the same current I_W. The geometry of the arrangement is shown in Figure 6. We assume that there are N_W such wires along the circumference. α_j is the angle of the jth wire (w.r.t the x axis) from the center of the beam pipe. From the field of an infinitely long wire it follows that the field at an anti-proton with coordinates (x, y) due to these wires is

$$B_y + iB_x = \frac{\mu_0}{2\pi} I_W \sum_{j=1}^{N_W} \sum_{n=0}^{\infty} [-\cos(n+1)\phi_j + i\sin(n+1)\phi_j] \left[\frac{(x+iy)^n}{r_j^{(n+1)}} \right] \tag{7}$$

where

$$\begin{aligned} r_j &= [(r_C \cos\alpha_j - r_{\bar{p}} \cos\theta_{\bar{p}})^2 + (r_C \sin\alpha_j - r_{\bar{p}} \sin\theta_{\bar{p}})^2]^{1/2} \\ \phi_j &= \arctan\left[\frac{(r_C \sin\alpha_j - r_{\bar{p}} \sin\theta_{\bar{p}})}{(r_C \cos\alpha_j - r_{\bar{p}} \cos\theta_{\bar{p}})} \right] \end{aligned} \tag{8}$$

Here r_C is the radius of the cage measured from the center of the beam-pipe, $(r_{\bar{p}}, \theta_{\bar{p}})$ are the distance and angle respectively of the anti-proton beam also from the center of the beam

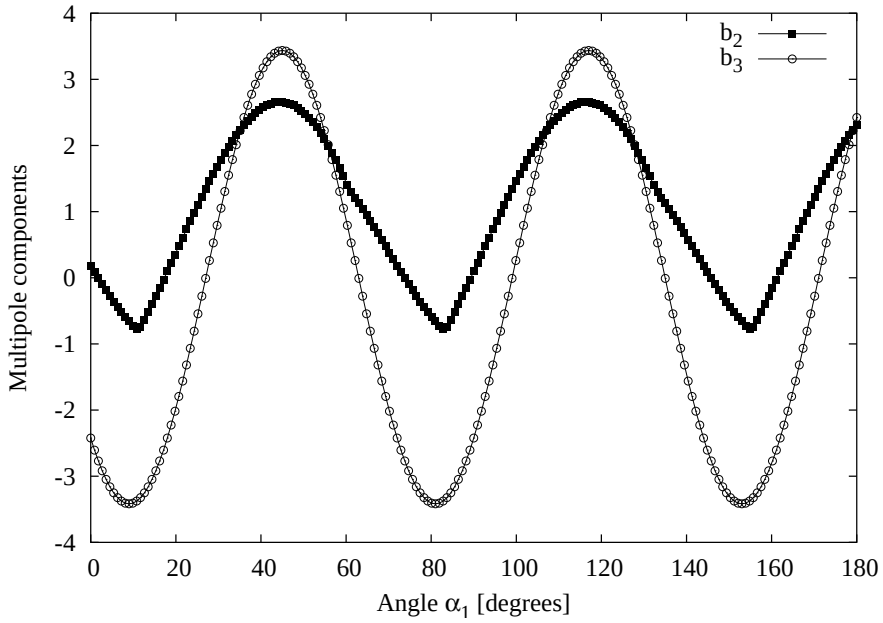

Figure 7: Normal sextupole and octupole coefficients (b_2, b_3) due to 5 wires placed uniformly around the beam vs the orientation angle of the wires.

pipe. Comparing this with the usual multipole expansion

$$B_y + iB_x = B_0 \sum_{n=0}^{\infty} (b_n + ia_n) \left[\frac{x+iy}{R_{ref}}\right]^n \tag{9}$$

we can write the multipole coefficients as

$$b_n = -\sum_{j=1}^{N_W} \cos(n+1)\phi_j \left[\frac{\langle r_W \rangle}{r_j}\right]^{n+1} \quad , \qquad a_n = \sum_{j=1}^{N_W} \sin(n+1)\phi_j \left[\frac{\langle r_W \rangle}{r_j}\right]^{n+1} \tag{10}$$

where the main field B_0 and reference radius $\langle r_W \rangle$ are

$$B_0 = \frac{\mu_0}{2\pi} \frac{I_W}{\langle r_W \rangle} \, , \qquad \langle r_W \rangle = \frac{1}{N_W} \sum_j r_j \tag{11}$$

We use these expressions to calculate the multipole coefficients as a function of the orientation of the wires. We let α_1 be the smallest angle of the wires w.r.t the anti-proton beam and assume (again for simplicity) that all other wires are distributed uniformly in azimuth, i.e. spaced at an angle $= 2\pi/N_W$ apart.

Figure 7 shows the variation in the normal sextupole and octupole components (b_2, b_3) as a function of the angle ϕ_1. We used $N_W = 5$ and chose the plane of the helix to be at 45°. We remark on some features: (i) the magnitude of each component varies by a factor of two to three as the angle is varied, (ii) the ratio of these components also changes with the

angle. Another feature not shown here is that the ratio of these components also depends on the number of wires, e.g. with 3 wires, the sextupole components are larger.

These aspects of the fields with multiple wires will allow greater flexibility in compensating selected resonances. We envisage a cage with several wires but powering only those wires at each location (depending on the orientation of the helix for example) which improve the lifetime. This investigation is still in a preliminary stage. Many more issues, such as the influence on the proton beam etc. need to be considered in a more detailed study.

References

[1] J.P. Koutchouk, *Principle of a correction of the long-range beam-beam effect in LHC using electromagnetic lenses* , LHC Project Note 223 (2000)

[2] J.P. Koutchouk, personal communication

8 Concluding Remarks

The following major problems need to be addressed in Tevatron to achieve the Run II luminosity goal: (1) diminishing the effects of Tevatron transverse head-tail instability, (2) increasing the beam separation at all stages of collider operation, and (3) suppression of the emittance growth during beam transfers and acceleration.

1. Diminishing the effects of Tevatron transverse head-tail instability implies the following steps:

   - Decrease of Tevatron transverse impedance by shielding the injection lambertson during 2003 summer shutdown;
   - Introducing cubic non-linearity into Tevatron focusing aimed to stabilize the head-tail instability at chromaticities close to zero;
   - Study of other possibilities to reduce Tevatron impedance (RF cavities, separators, etc.) It should allow operating collider with zero chromaticities with a consequent reduction of particle loss at injection, acceleration, squeeze and collisions.

2. Increasing the beam separation requires the following:

   - Better optimization of helical orbits at all stages of collider operation;
   - Finding and removing limitations of physical and dynamic apertures;
   - An increase of separator strength for near IP separators to increase beam separation at collisions. A required 40% increase of separator strength can be achieved by utilizing the space where presently unused Q1 quads are located and, in a lesser degree, by voltage increase;
   - We are presently studying a possibility to coat the separator plates so that to increase their electric field;
   - In order to make the best use of present set of separators, it is important that all separators are equipped with polarity reversal switches, and their conditioning needs to be done closer to their maximum voltages (∼130-150 kV), so that they could be used at higher voltages during short time of acceleration and squeeze.

     It should minimize harmful effects of parasitic collisions and should allow operation with higher intensity beams.

     A simple and reliable way to address the problem of nearest to IP parasitic collisions is to increase distance between bunches. A larger distance eventually will require smaller number of bunches, and, consequently, smaller total longitudinal emittance of the antiproton stack in Accumulator (or Recycler). Taking into account that presently we already see limitations coming from large longitudinal emittance of antiproton stack the drastic reduction of bunches (factor of two or comparable) does not look promising. Nevertheless even small increase of bunch-to-bunch distance from 21 to 23 RF buckets would be sufficient. It can be achieved

by rearranging transfers from MI to Tevatron and modification of MI antiproton kicker. Adding one bunch at both ends of every proton train can also significantly alleviate the beam-beam effects for antiproton bunches #1 and #12 of every antiproton train.

3. Suppression of the emittance growth during beam transfers and acceleration requires minimization of injection errors and optics mismatches:

   - To minimize injection errors the special turn-by-turn turn BPMs (beam line tuners) are used for tuning orbit closure. After completion of their commissioning in summer 2003, additionally to the presently reported injection errors they will be reporting betatron tunes, coupling and a few other important parameters for every bunch injected in Tevatron. Additional suppression of the emittance growth should come from the injection dampers scheduled to be commissioned in the fall of 2003.
   - Suppression of optics mismatches between Main Injector and Tevatron is still a pending problem. Present understanding is that the strong coupling in Tevatron drives this mismatch. Therefore solving this problem will require careful optics control and correction for Tevatron and MI-to-Tevatron transfer lines.
   - Particles with large synchrotron amplitudes are very susceptible to the beam-beam effects and machine non-linearities. Therefore it is important to prevent longitudinal emittance growth in the entire chain of accelerators.

Further improvement in the beam instrumentation is the key to the improvement of the machine performance. The major items are:

- New 1.5 GHz Shottky monitor is presently under commissioning and is expected to measure tunes and chromaticities for each proton/antiproton bunch;
- Measurements of tunes, coupling and chromaticities based on the turn-by-turn measurements of head-tail dynamics after bunch transverse kick is under development;
- Ionization profile monitor is presently under development and should be capable to measure the turn-by-turn bunch sizes. It is expected that it will be extremely useful for diagnostics of optics mismatches for MI-to-Tevatron transfers;
- On-line magnetic measurements of dipole and multipole content for Tevatron superconducting dipoles, and measurements of magnetic field fluctuations;
- Planned improvements of BPM system should allow to measure beam positions during the store, and to perform more accurate differential orbit measurements and turn-by-turn measurements.
- Improvements in optics measurements and their analysis should allow carrying out fast and effective diagnostics of Tevatron optics.

- It is highly desirable to have a tune feedback, which would be stabilizing tunes to the about 0.001.
- On-line measurements of motion/displacements for magnets and tunnel floor (seismic, slow drifts)

After many years of operation Tevatron dipoles got a systematic roll due to motion of the tunnel floor, and systematic skew-quadrupole fields due to coil displacement relative to the dipole iron core. It is desirable to correct all large rolls of the dipoles. It would be good to correct the skew-quadrupole in all dipoles. However it is not really required. It would be sufficient to correct it for a small fraction of dipoles, which do not have nearby skew-quadrupole.

We are working now on an active compensation of beam-beam effects by the electron lens. It is a challenging project, but if it will be successful it should allow achieving higher values of beam-beam tune shift and, consequently, higher luminosity.

Shortening of shot setup time will yield smaller losses at injection and larger luminosity integral.